Three-dimensional Super-resolution Imaging of Live Cells

Sara A. Jones, Sang-Hee Shim, Jiang He and Xiaowei Zhuang

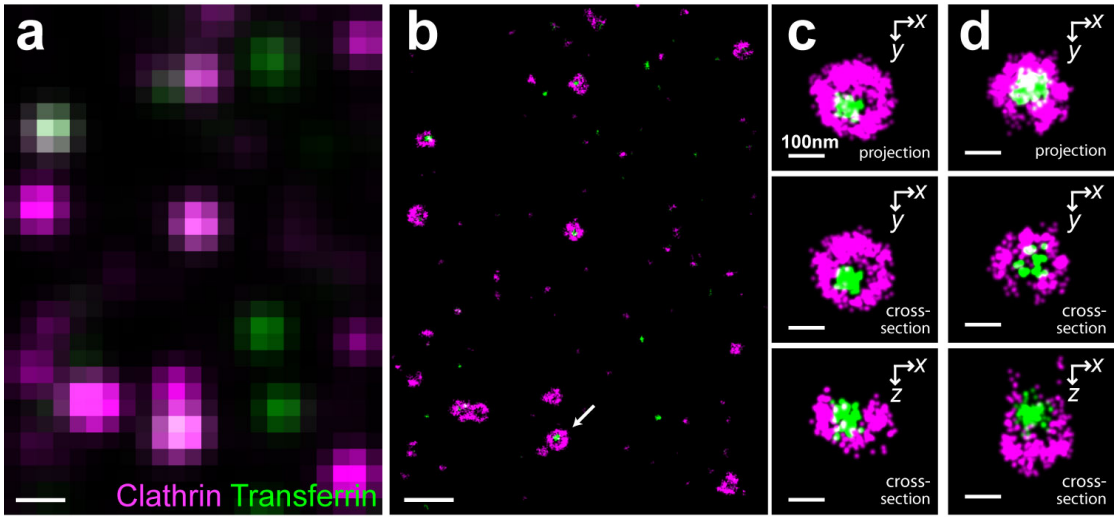

Supplementary Figure 1: STORM images of transferrin and clathrin in a fixed cell. (**a**) Conventional image of transferrin (green) and clathrin (magenta). Transferrin is directly conjugated with Alexa405 and Alexa647 and the clathrin heavy chain is immunostained with secondary antibodies labeled with Cy3 and Alexa647. In this scheme, the photoswitchable reporter Alexa647 was imaged and the probes were distinguished by the wavelength of activation light. (**b**) STORM image of the same area. The *xy* projection of the 3D image is shown. (**c**) 3D STORM images of an example CCP taken from **b** (indicated by the arrow). Top row: *xy* projections. Second row: *xy* cross-sections near the plasma membrane. Bottom row: *xz* cross-sections cutting through the middle of the pit. (**d**) 3D STORM images of a CCP containing transferrin labeled with Alexa568. Clathrin heavy chain is immunolabeled labeled with Alexa647. In this scheme, the two photoswitchable dyes, Alexa568 and Alexa647, were distinguished by their emission spectra. Top row: *xy* projections. Second row: *xy* cross-sections near the plasma membrane. Bottom row: *xz* cross-sections cutting through the middle of the pit. In all figures, the *z* axis points away from the glass substrate. Scale bars, 500 nm (**a**,**b**), 100 nm (**c**,**d**).

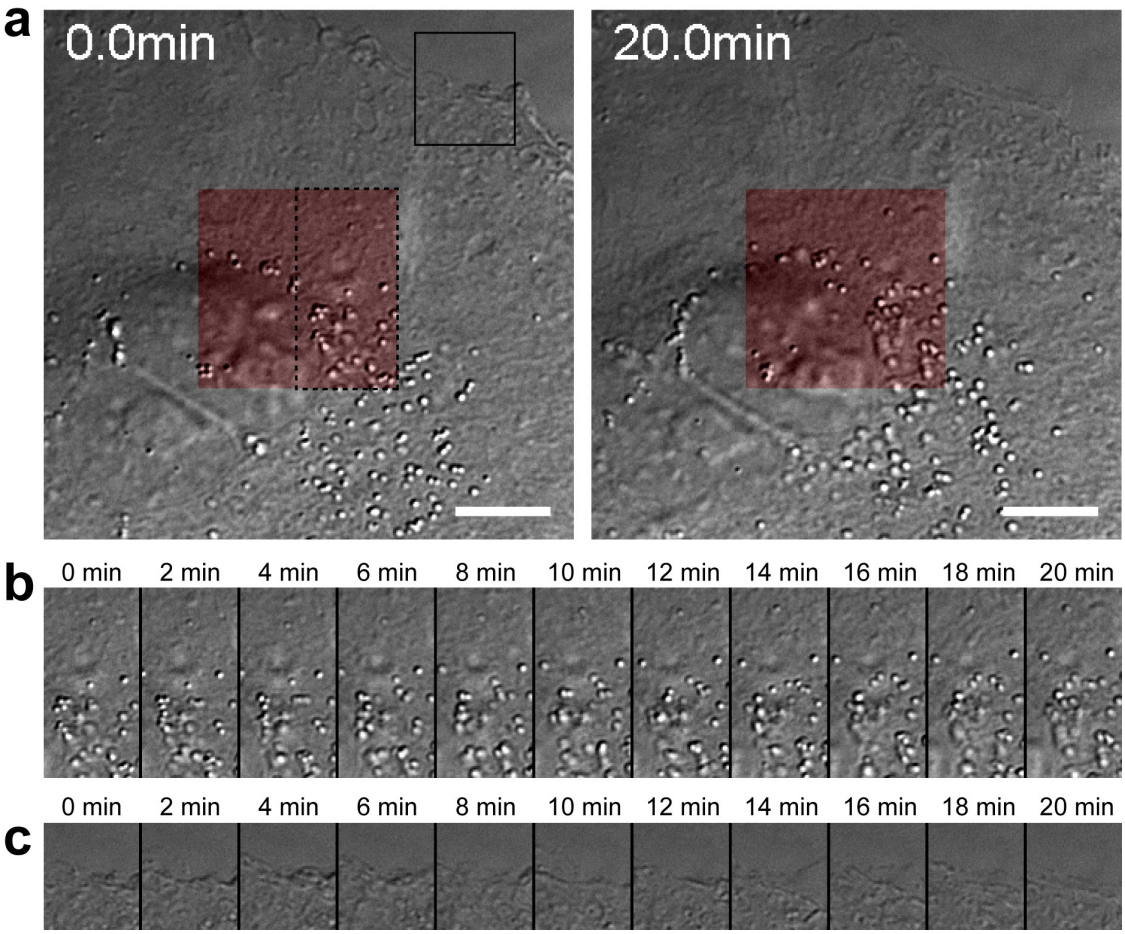

Supplementary Figure 2: DIC images of a cell under the STORM imaging conditions. (**a**) A BS-C-1 cell was placed in imaging buffer at 34°C and continuously irradiated for 20 minutes with 15 kW/cm^2 of 657nm laser. The 657 nm laser was turned on immediately prior to the start of DIC imaging. The red area corresponds to the illuminated region of the cell, which is equivalent to the typical beam size used in STORM experiments (20 μm x 20 μm). A larger region of the cell encompassing the illumination area is shown to display the cell morphology. The regions in the dashed box (**b**) and solid box (**c**) are shown at various time points to highlight the observations that both the intracellular vesicles continue to move and cell edge probes its environment throughout the imaging time. We note that STORM experiments in this work were typically 2-3 minutes in length, and many did not require the maximum 15 kW/cm^2 excitation intensity. The entire 20-min course of the full field is provided as Supplementary Movie 1. Scale bar, 10 μm (**a**).

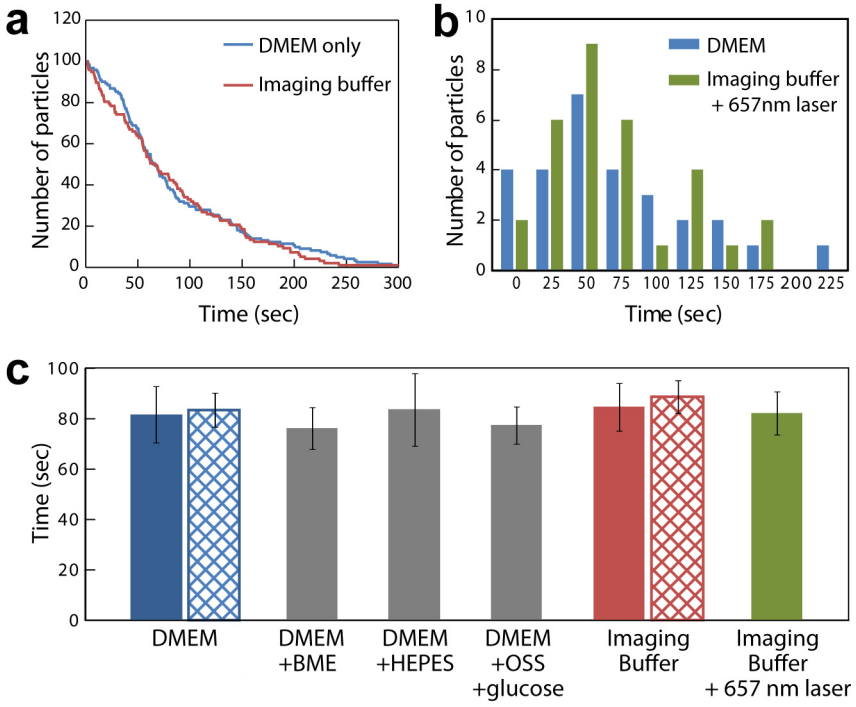

Supplementary Figure 3: Comparison of transferrin uptake kinetics under various buffer and illumination conditions. To test whether the additional buffer components for STORM imaging and the strong laser illumination used for the fast STORM imaging induced adverse effects on transferrin uptake, Cy3-labeled transferrin was added to live cells at 34°C and transferrin uptake was probed in various buffer compositions, and in the presence and absence of the 657 nm illumination (15 kW/cm^2). A low intensity 561 nm light was used to image the Cy3-labeled transferrin in the total internal reflection (TIRF) or oblique incidence geometry. Photobleaching due to the weak 561 nm illumination was negligible during the course of imaging. (**a**) The number of transferrin puncta on the cell surface as a function of time measured using TIRF imaging geometry. Due to the limited imaging depth of the TIRF field, as the transferrin clusters were internalized and left the TIRF illumination field, the number of transferrin clusters on the cell surface decreased over time, providing a measure of uptake kinetics. The total number of clusters at time zero was normalized for comparison. Similar uptake kinetics were observed in Dulbecco's Modified Eagle Medium (DMEM) and in the DMEM-based imaging buffer supplemented with 6.7% of 1M HEPES pH 8.0, 0.5% beta-mercaptoethanol (BME), 2% glucose and an oxygen scavenging system (OSS) as described in the Methods section. (**b**) As an alternative approach to probe for transferrin internalization, we

tracked the movement of individual transferrin clusters using the oblique-incidence imaging geometry. Typically, the clusters moved on the cell surface slowly, but after internalization, the transferrin-containing vesicles exhibited rapid and directed microtubule-dependent movement (as confirmed by the use of a microtubule-disrupting drug, nocodazole). Shown in the plot are the distributions of the lag time between the start of the movie and the beginning of microtubule-dependent motion. To dissect potential effects of various components in the imaging buffer, we measured the transferrin uptake kinetics using this approach under various buffer conditions (DMEM, DMEM with BME, DMEM with HEPES buffer, DMEM with glucose and OSS, and imaging buffer containing everything above). To assess the effect of the strong 657 nm illumination, we further measured the transferrin uptake kinetics in the imaging buffer both in the presence and absence of the 657 nm illumination. Here the lag time distributions observed in DMEM without the 657 nm illumination and in the imaging buffer with the 657 nm illumination are shown. (**c**) Summary of the transferrin uptake time measured in 6 different buffer compositions, and in the absence and presence of the 657 nm illumination. The cross-hatched bars are derived from measurements described in (a) and solid bars are derived from measurements described in (b). The various conditions are: (1) DMEM only; (2) DMEM with 0.5% BME; (3) DMEM with 6.7% 1M HEPES pH 8.0; (4) DMEM with 2% glucose and OSS; (5) Imaging buffer comprised of DMEM with 6.7% 1M HEPES pH 8.0, 0.5% BME, 2% glucose, and OSS; (6) Imaging buffer with 15 kW/cm^2 657 nm illumination. In all cases, we find the internalization rates to be consistent with those observed in the standard DMEM buffer without 657 nm illumination, indicating that our imaging buffer and illumination conditions did not exert significant effects on the uptake of transferrin.

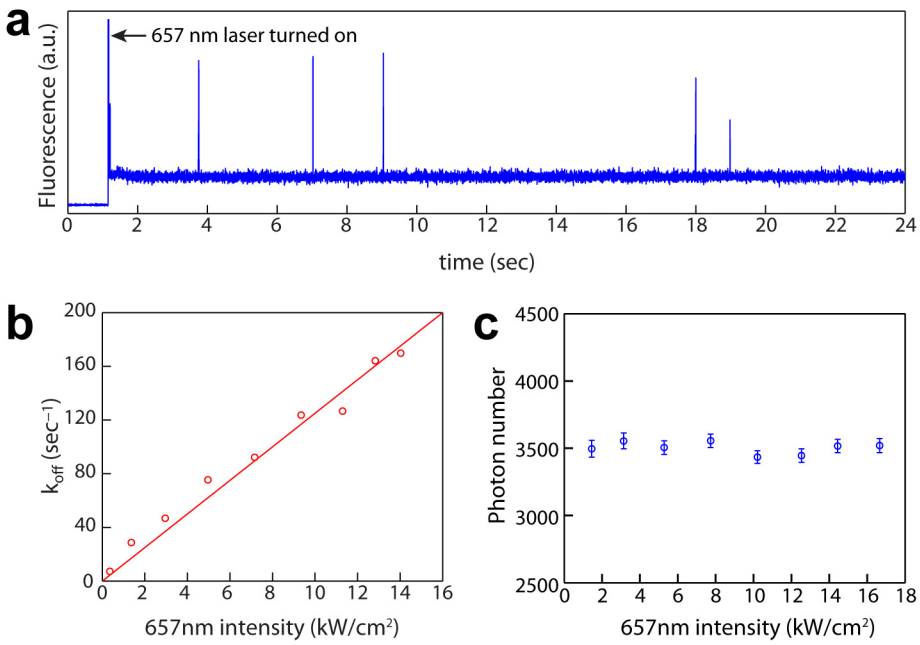

Supplementary Figure 4: Photoswitching kinetics and number of photons detected per switching cycle of Alexa647. (**a**) The switching trace of a single Alexa405-Alexa647-labeled transferrin molecule under 405 nm and 657 nm illumination. (**b**) The dependence of the rate constant for switching off Alexa647 (k_{off}) on the 657 nm excitation intensity. Circles represent experimental data and the line displays the corresponding linear fit. (**c**) The average number of photons detected per photoswitching cycle of Alexa647 measured at various 657 nm laser intensities.

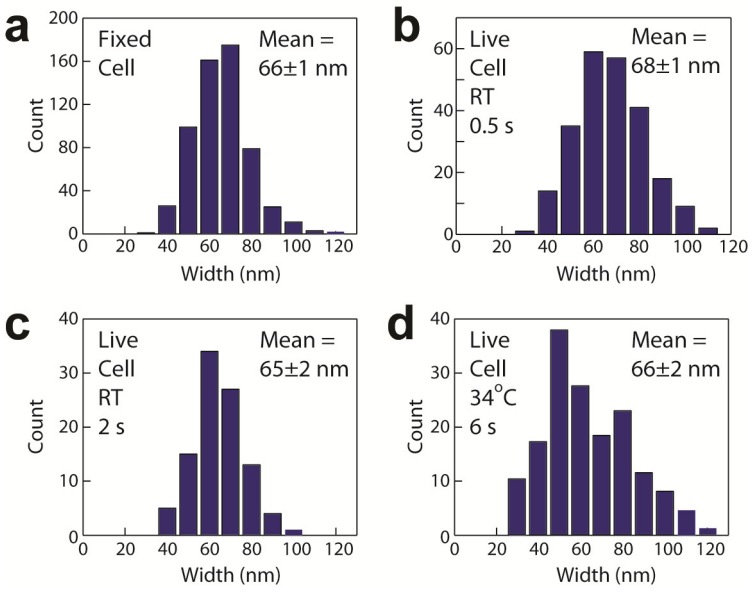

Supplementary Figure 5: Size distributions of transferrin clusters measured from fixed-cell and live-cell STORM images. To measure the size of each individual structure, histograms were generated from the *x* and *y* positions of localizations within the structure and fit with a Gaussian to obtain the full-width half maximum. The widths of many individual structures were determined and plotted in the above histograms. Transferrin cluster sizes in (**a**) fixed-cell images, (**b**) live-cell 0.5-sec snapshots at room temperature, (**c**) live-cell 2-sec snapshots at room temperature and (**d**) live-cell 6-sec snapshots at 34°C are shown.

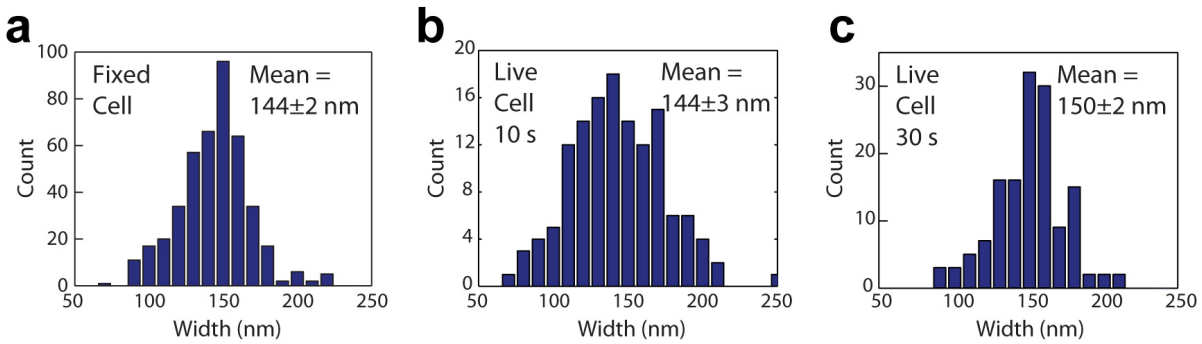

Supplementary Figure 6: Size distributions of clathrin-coated pits measured from fixed-cell and live-cell STORM images. To measure the size of each individual structure, histograms were generated from the *x* and *y* positions of localizations within the structure and fit with a Gaussian to obtain the full-width half maximum. The widths of many individual structures were determined and plotted in the above histograms. Lateral dimension of CCP in (**a**) fixed-cell images, (**b**) live-cell 10-sec snapshots and (**c**) live-cell 30-sec snapshots at room temperature are shown.

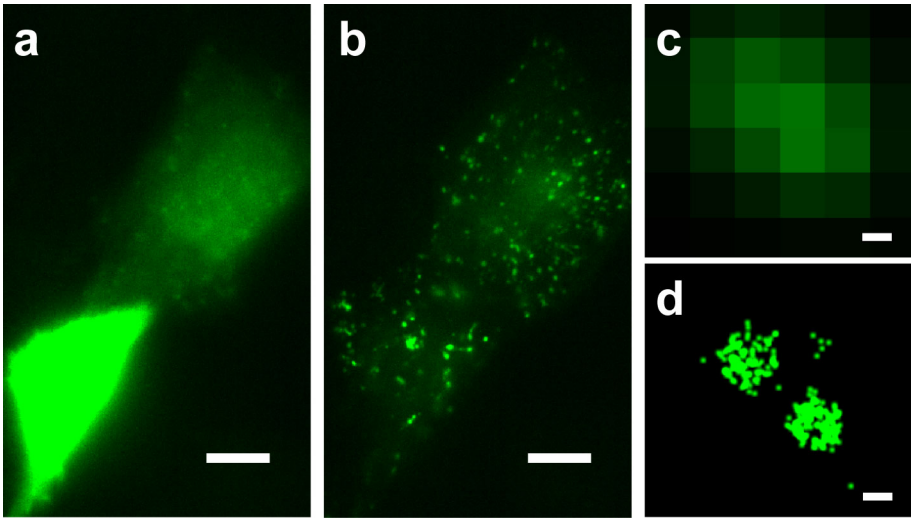

Supplementary Figure 7: Live-cell delivery of the Alexa647 dye for STORM imaging by the bead-loading approach. By sprinkling glass microbeads onto cells to temporarily disrupt the plasma membrane and subsequently removing the beads to allow cell recovery, dye molecules in the medium can be delivered into the cells while maintaining cell viability[36]. Using this approach, we have successfully loaded SNAP-reactive Alexa647 (BG-Alexa647) and labeled the SNAP fusion proteins of clathrin in live cells. (**a**) Conventional image of cells immediately after bead loading showing diffuse dye molecules. (**b**) Conventional image of the same area after ~50 min shows punctate clathrin structures labeled with Alexa647 and removal of excess dyes by endogenous cellular transporters. A zoom-in conventional image (**c**) and the STORM image of the same area (**d**) illustrate the substantially improved resolution by STORM. Scale bars, 10 μm (**a**,**b**), 100 nm (**c**,**d**).

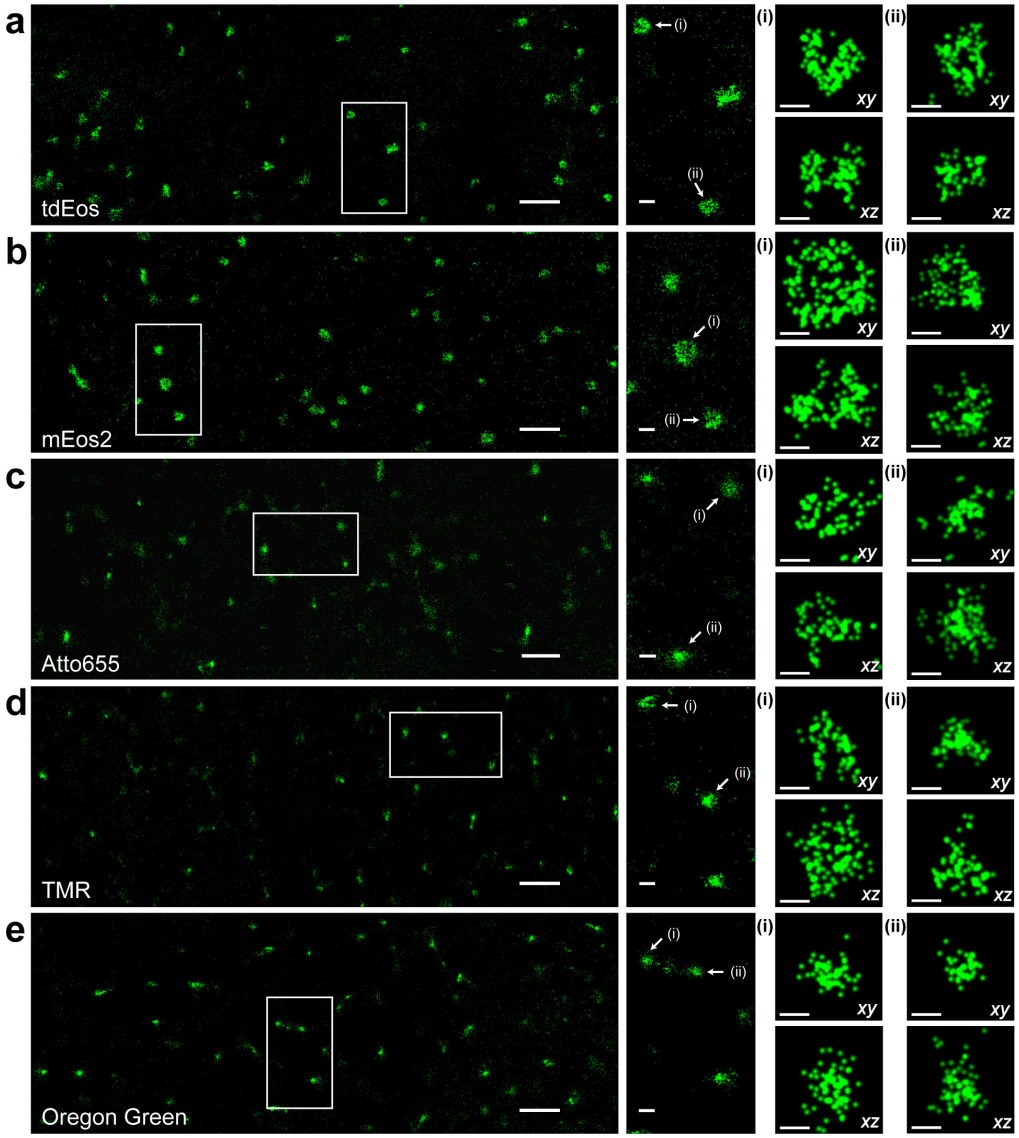

Supplementary Figure 8: 3D STORM images of clathrin-coated pits tagged with tdEos (a), mEos2 (b), Atto655 (c), TMR (d) and Oregon Green (e) in live cells. Clathrin light chain was labeled with these probes either directly (tdEos and mEos2) or through a SNAP tag (Atto655, TMR and Oregon Green). Left most column: 3D STORM images of a large field of view. The *xy* projections of the 3D images are shown. Second left column: A zoom-in of the boxed regions in the larger images. Two right columns: The *xy* and *xz*-cross sections of the two CCPs indicated with arrows in the second left column. The large-field images displayed above are a portion of the full-frame images (either 20x20 μm or 20x40 μm), which in turn were used to generate the composite CCP image shown in **Figure 4** and the resolution characterizations in **Supplementary Table 1**. Scale bars, 1 μm (left most column), 200 nm (second left column), 100 nm (two right columns).

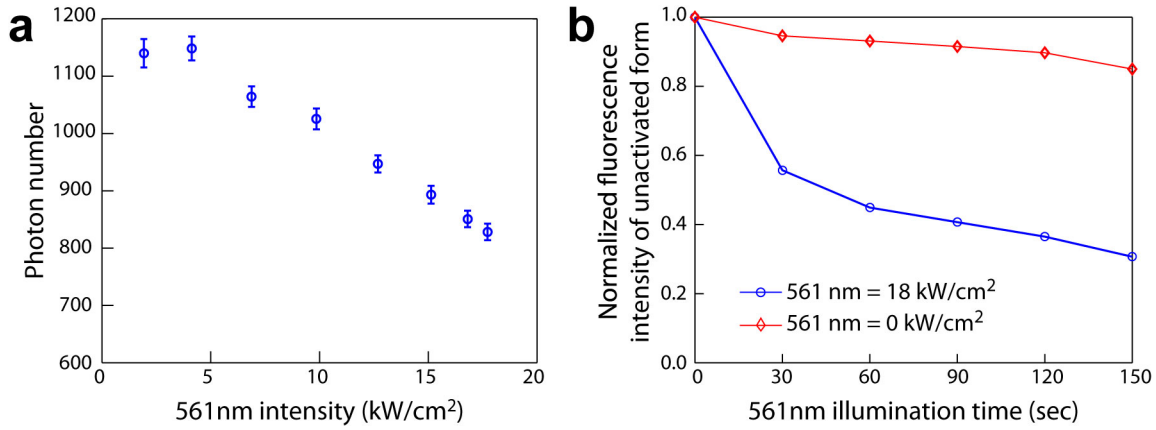

Supplementary Figure 9: The effects of the excitation light on the number of photons detected from activated mEos2 and on the photobleaching of unactivated mEos2. BS-C-1 cells were transiently transfected with non-targeting mEos2, fixed, and imaged for the measurements. (**a**) The average number of photons detected from single molecules of mEos2 after activation (by 405 nm illumination) until photobleaching, measured at various 561 nm excitation laser intensities. (**b**) Ensemble fluorescence intensity of mEos2 prior to activation with 405 nm light. The fluorescence signals were measured with 460 nm excitation while the cell was repeatedly illuminated with 561 nm light (30 sec exposures) between consecutive 460 nm imaging. Without the 561 nm illumination (red curve), the fluorescence of unactivated mEos2 decreased slightly due to photobleaching by 460 nm laser. Upon illumination with the 561 nm laser, significantly more unactivated mEos2 was bleached, increasing with the 561 nm illumination time (blue curve).

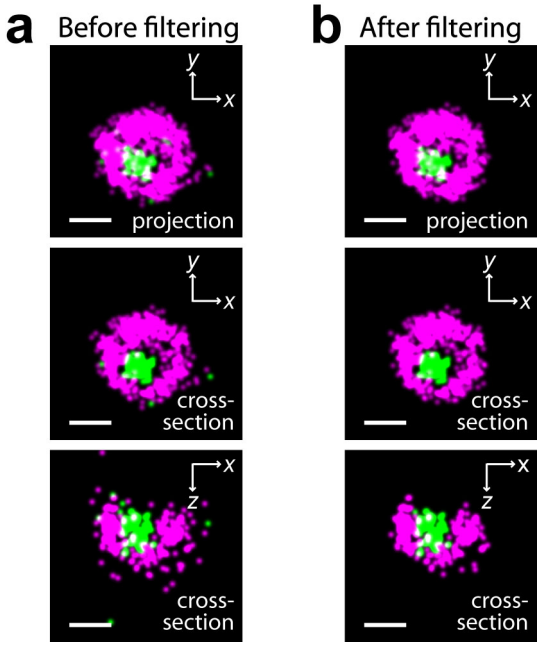

Supplementary Figure 10: Comparison of STORM images before and after local density filtering. Shown here are two-color 3D STORM images of a CCP (magenta) containing transferrin (green). (**a**) Images prior to density filtering. (**b**) Images after local density filtering as described in the Methods section. Top row: *xy* projections. Second row: *xy* cross-sections near the plasma membrane. Bottom row: *xz* cross-sections cutting through the middle of the pit. The images after density filtering are also presented in **Supplementary Fig. 1c**. Scale bars, 100 nm.

Supplementary Table 1: Comparison of the spatial resolution characteristics of Alexa647, tdEos, mEos2, Atto655, TMR and Oregon Green measured in the live-cell STORM experiments. Localization precisions are measured in full-width at half maximum (FWHM). Convolved resolutions are computed as $[(\text{Localization precision})^2 + (\text{Nyquist resolution})^2]^{1/2}$. The detected photon numbers in each switching cycle typically follows an exponential distribution. A cutoff value of 500 photons is used to screen switching events to avoid localizations with large uncertainty. Localization precisions are reported here as the average values within the imaging depth of 300 nm. The variation in localization precision at different *z* is moderate (See Methods for a quantitative description). Errors in localization numbers, given as standard deviation of *n* measurements from *n* CCPs, are propagated to the Nyquist resolutions.

Probe	**Alexa647**	**tdEos**	**mEos2**	**Atto655**	**TMR**	**Oregon Green**
Average photon number per switching cycle	~3500	~1200	~1200	~1200	~1100	~900
Localization precision in *xy* (in FWHM)	17 nm	27 nm	27 nm	27 nm	28 nm	30 nm
Localization precision in *z* (in FWHM)	45 nm	71 nm	71 nm	71 nm	74 nm	81 nm
Localization number per CCP in a 30-sec snapshot	~450 ± 150 (*n* = 30)	~250 ± 70 (*n* = 29)	~230 ± 110 (*n* = 26)	~190 ± 90 (*n* = 37)	~150 ± 70 (*n* = 23)	~90 ± 50 (*n* = 23)
3D Nyquist resolution	24 ± 3 nm	29 ± 3 nm	30 ± 5 nm	32 ± 5 nm	35 ± 5 nm	41 ± 7 nm
Convolved *xy* resolution	29 nm	40 nm	40 nm	42 nm	45 nm	51 nm
Convolved *z* resolution	51 nm	77 nm	77 nm	78 nm	82 nm	91 nm